I. Introduction

Amorphous TiO_2 thin films are used in many optical applications because of the materials high index of refraction, and corrosion resistance [1,2]. Reactively sputtered TiO_2 has a low deposition rate compared to other sputtered oxides. The deposition rate can be increased using feedback loops combined with inert gases [1, 3-5]. TiO_2 sputtered at room temperature is amorphous at relatively high deposition rates. A drawback of amorphous TiO_2 is a low crystallization temperature, around 300 ^oC [6-8]. This is a concern in coatings where post-processing temperatures exceed the crystallization temperature [3]. TiO_2 has three crystalline phases (anatase, rutile, and brookite) each with differing optical properties [9-11]. The phase stability at high temperatures is crucial for the heat treatment of thin film coatings employing amorphous TiO_2, for example, coatings deposited on float glass before a tempering process, ranging from 650^{o}C to 730^{o}C.

Nitrogen added to a TiO_2 process has the effect of improving film thickness uniformity across substrates. Adhesion of epitaxial and polycrystalline TiO_2 films can be increased by implantation of N ions [12]. Nitrogen also has the effect of making the film absorbing and reducing the optical transmittance. As a result, nitrogen is used sparingly. Recent work concerning titanium oxynitride has focused on the addition of oxygen into TiN films, and thus investigates film properties with high concentrations of nitrogen [12-14]. TiN coatings are mostly

used as strong protective coatings and as absorbent optical coatings. In this paper we focus on the crystallization kinetics of TiO_xN_y films where x is much larger than y.

We investigate the effect of nitrogen addition on the crystallization kinetics of TiO_2 using the Johnson-Mehl-Avrami-Kozolog (JMAK) equation, which is traditionally used to model crystallization and growth from an amorphous phase [15-17]. This formalism was developed for isothermal, random nucleation, which is satisfied in our experiments.

Our research has shown an increase in the nucleation temperature occurs in TiO_2 with little change in the optical properties, when nitrogen is added to the sputtering process gas. In this case the nucleation temperature is defined as the temperature at which rapid nucleation and growth occurs in an experiment, for a time scale on the order of a few minutes. Nitrogen has been shown to play the role of an amorphous stabilizer in certain alloy systems; it appears to have the same qualities in the TiO_2 system [18]. Two analyses are performed in this paper that result in similar values for the kinetic variables. The kinetic variables extracted from the nucleation and growth of individual crystallites are used as inputs in the JMAK equation as a sensibility check. Finally, the predicted fraction transformed from the kinteic variables and a measure of the nucleation rate is compared to experimental results.

1. Experimental

Ten specimens 50 nm thick were prepared using increased nitrogen content in the reactive gas (two samples for each nitrogen content). The TiO_xN_y films were sputter deposited from a titanium target in an oxygen/nitrogen reactive atmosphere onto amorphous silicon nitride transmission electron microscope (TEM) membranes. The base pressure of the system was on the order of 10^{-6} torr. The process gas was a mixture of Ar, N_2 and O_2 totaling 50 sccm, for a pressure of approximately 3 mtorr. The argon flow was held constant at 32 sccm and the remaining 17 sccm a mix of oxygen and nitrogen (0-5 sccm or 0-40 % of oxygen flow). A power density of 7.895 W/mm was used with a target to substrate distance of 6 mm. The film was deposited on glass slides and the thickness was determined optically using W-VASE^{TM} software and the modified Conrady model for dielectrics. The band gap energy was determined from Tauc analysis of the optical constants [19].

The kinetic analysis was performed at the National Center for Electron Microscopy (NCEM) at Lawrence Berkeley National Laboratory (LBNL) using a JEOL 200 CX *in-situ* TEM with a LaB_6 filament operating at 200 keV. The sample is placed in a tantalum furnace that is heated resistively. The furnace temperature is determined by a K-type platinum/platinum-13% rhodium thermocouple affixed to the body of the furnace. The TEM holder used is a Gatan Inc. Model 652-Ta double-tilt heating holder able to ramp to any

temperature below 1300 ^{o}C in 60 seconds, and the temperature can be determined to within 10 ^{o}C. The amorphous state of the as-deposited film was verified by inspection of the diffraction patterns. Diffraction patterns were taken after crystallization to determine phases present and any preferential grain orientation.

The annealing temperature varied from 250 ^{o}C to 400 ^{o}C for 2-3 minutes. The specimens were heated in 25-degree increments until nucleation was observed, the temperature was then dropped 50 degrees for growth data. Growth consistently occurs at temperatures lower than the onset of nucleation, after nucleation has begun. The samples were then ramped in 10-degree increments for 5-minute periods until the sample had completely crystallized.

Image analysis of videotape was used to extract the kinetic variables. In each of the regions observed 2-5 nucleation sites were followed and the area of each site was determined as a function of time. It was assumed that the grains were circular, which is approximately true. Kinetic variables were extracted as well as the fraction of material transformed at 400 ^{o}C. For the fraction transformed analysis, the nucleation rate was determined by counting the number of crystallites visible in a time increment and dividing by the untransformed area. The fraction of crystallized volume was determined by image analysis.

III. Data

The first observation on the TiO_2 samples made with increased nitrogen is that the deposition rate also increased. This trend can be seen in Figure 1, where the thickness *d* relates to the dynamic deposition rate (DDR):

$$d = DDR\left(\frac{Power}{length}\right) \times \frac{\#passes \times \#cathodes}{linespeed} \quad (1)$$

The increase in DDR is not surprising because as nitrogen was added oxygen was removed, and the operating point relocated to a more metallic region of the hysteresis curve. When oxygen was taken out of a pure oxide plasma it transitioned to metallic mode at a higher flow rate than with a mixed oxygen/nitrogen plasma. This shows that the nitrogen acts as a stabilizer so operation is allowed with the target surface at a more metallic state. Chemically, Ti prefers to react with oxygen, which may make the nitrogen effectively inert.

Optical analysis revealed that the changes made in the nitrogen content did not greatly increase the absorption of the film. The index of refraction and extinction coefficient values can be seen in Table 1. The observed index of refraction decreases minimally. The slight change in the extinction coefficient indicates that the plasma stays in the oxide mode and that little to no TiN, which has high

absorption and metallic conductivity, is being deposited. It was not possible to determine whether the optical band gap was direct or indirect with Tauc analysis, however, the band gap energy remains fairly constant with similar values for either case. The slight decrease can be explained by noting that increased nitrogen in the process gas increases the deposition rate causing more disorder the TiO_2 film.

The corners of all TEM grids were amorphous although the centers of some samples were crystallized. The indexing of the diffraction patterns can be seen in Figure 2. From the diffraction patterns the phase of the amorphous films after crystallization was determined to be anatase or brookite, since both share the diffraction rings found in the samples. The rutile and TiN phases were safely excluded. The diffraction patterns of as-deposited crystalline films, with low nitrogen incorporation, revealed the same rings as post crystallization as seen in Figure 2. Films deposited on glass slides were baked at 400^oC and the index of refraction for the film dropped from 2.4 to 2.3 at 550 nm wavelength. This value is much closer to anatase (2.48-2.56) than brookite (2.58-2.7), and thus the majority of the film is anatase [10-11]. Based on single crystal diffraction patterns of isolated crystallites there was no preferential growth of any crystallographic orientation. As the nitrogen content decreased, the amount of as-deposited crystallized phase in the TEM grid centers increased, which is consistent with the kinetic data presented in this paper.

The nucleation temperature of the amorphous films at the TEM grid edge increased with increasing nitrogen content, as can be seen in Figure 3. This was the first indication that the nitrogen had an effect on the crystallization kinetics. The grain growth rate was found to be constant during isothermal annealing in the temperature range of 300-500 ^{o}C.

Figure 4 displays the grain growth data collected and the linear approximations used to extract the kinetic exponents. The slope indicates the activation energy and the intercept indicates the growth velocity at infinite temperature. These values can be used with Equations 2 and 3 to model the fraction transformed. It is important to note that the sample with no nitrogen has a much higher slope and is completely crystallized before any sample with nitrogen starts the crystallization process. This indicates that there is less resistance to nucleation and growth with the absence of nitrogen in the process gas.

The differences between films are very apparent when comparing the pre-exponential velocity, $v_{o,}$ with increasing temperature, as seen in Figure 5. Note that all of the samples with nitrogen approach a similar velocity at a high temperature. In addition, the sample with no nitrogen is expected to have a much higher velocity at the elevated temperature. This is significant in that only a slight addition of nitrogen into the reactive atmosphere decreases crystallization velocity significantly.

In Figure 6 the activation energy, Q_{kin} , as a function of the nitrogen can be seen. The activation energy is an indicator of the effect of the nitrogen on the matrix. Kinetic data is shown in Table 2. With no nitrogen the activation energy is 1.96 eV. With a nitrogen mixture of 13% the value drops to 1.5 eV. As more nitrogen is added the activation energy decreases further. With no nitrogen, the Ti and oxygen atoms have more mobility. The addition of nitrogen seems to act as a diffusion inhibitor and limits the movement of Ti and oxygen. This is clearly evident in the crystal growth velocity data at 730 ^{o}C, as seen in Figure 7.

IV. Analysis and Discussion

It was noticed that growth occurs below the nucleation temperature, *after* nucleation. A possible explanation is that the activation energy for growth is lower than that of nucleation. When a sample reaches the growth temperature with no nucleated sites, no growth will occur. After the nucleation temperature is reached the growth mechanism takes over and large fast growing crystallites dominate the transformation. Above the nucleation temperature, accurate extraction of the growth kinetic variables is difficult, because of the fast growth. The energy required to grow the grains is lower than that to nucleate new growth sites. This can be explained by higher activation energy for the nucleation than for growth. This is also allows us to argue that there are no preexisting nucleation sites, since no growth occurred before the nucleation threshold was reached.

We will now compare our extracted kinetic variables, Q_{kin} and v_o from the analysis of individual crystallites, to the variables *n* and *k*, obtained from JMAK analysis of the entire film at a constant temperature of 400 ^{o}C. The JMAK equation is:

$$f(t) = 1 - \exp(-kt^n) \quad (2)$$

Where f represents the volume fraction crystallized after time *t*. The Avrami exponent (or mode parameter) from Equation 2 is $n = a+bp$. Here, *a* relates to the nucleation rate, which is 0 for pre-existing nucleation sites and 1 for no pre-existing sites and a constant nucleation rate. *b* indicates the dimensionality of the growth (1,2 or 3). *p* is associated with the kinetics of growth, having a value of 1 for interfacial controlled growth (or constant radial growth) and _ for curvature driven growth. The Arrhenius equation expresses the temperature dependence of *k* [20]:

$$k = k_o \exp\left(\frac{-E}{k_b T}\right) \quad (3)$$

Where k_o is a pre-exponential, k_b is Boltzman's constant, and *T* is temperature. Equation 3 can also be shown as Equation 4 for two-dimensional growth [18].

$$k = \frac{\pi}{3} N_r v^2 \qquad (4)$$

Here N_r is the nucleation rate and v is the growth velocity. In this case $v=v_o exp[-Q/kT]$ is thermally activated. So *ln(k) vs. 1/T* gives $E=2Q + \beta$ where β is the activation energy of nucleation.

A second analysis using Equation 2 allows the kinetic variables to be compared to parameters extracted from the fraction transformed data. By taking the natural log of $f(t)$ twice we get:

$$\ln(-\ln(1- f(t))) = \ln(k) + n\ln(t) \qquad (5)$$

The comparison of the fraction-transformed analysis at a constant temperature with the kinetic variables extracted from the growth analysis of individual crystallites is shown in Table 2. Since temperature is constant in the fraction transformed analysis, we do not need to know β, only N. The sample with no nitrogen crystallized so quickly that counting nucleation sites was impossible - obviously there was a much higher nucleation rate than the other samples. For this sample, the nucleation rate was adjusted so that the value of k was nearly the same for both analyses. The nucleation rate we arrive at was found to be significantly higher than other samples, which agrees with experimental observations. Figure 8 shows the JMAK plot of each sample. k is derived from

exponential of the intercept of the curves. Note that the curves are stacked from highest to lowest N_2 ratio.

As stated earlier, there was no growth until a nucleation threshold temperature was reached, and growth did occur for each sample below each nucleation temperature, after nucleation. This indicates that crystallite nucleation in these films is homogeneous. In addition, *N* was found to be nearly constant at 400 ^{o}C, therefore, *a=1*. If it is assumed that the growth is radial which is approximately true, then *p=1* and *b=2* for 2-dimensional growth, since we are working with thin films. Initially there is some 3 dimensional growth because the crystallites need to grow through the film thickness, but this is insignificant in comparison to the 2 dimensional growth. This gives an approximate mode parameter of *n*=3; therefore the initial times were adjusted to get a value as close to 3 as possible. Nucleation, and thus some growth, occurs before the temperature of 400 ^{o}C is reached during the temperature ramp up time of about 15 to 30 seconds. The fact that the JMAK curves fit the data very well justifies the addition of a positive offset to the times.

The results from the JMAK fraction transformed analysis, Equation 5, agree very well with the nucleation and growth data from analysis of individual crystallites. The experimental results for the fraction transformed, and fits from Equation 5 using the n_{JMAK} and k_{JMAK} from columns II-III of Table 2, can be seen in Figure 9. Note that the nitrogen fraction increases the time to complete crystallization.

The most important comparison is the extraction of k_{JMAK} from Equation. 5 and a calculated k_{kin} from the kinetic data Q_{kin} , v_o and N from Equation 4. When k_{kin} is used in the JMAK Equation the differences in the fraction transformed look large, see Figure 10. However a change for each of the activation energies of only 2-6% from Q_{kin} to Q_{mod} is enough to have the resulting curves from Equations 2-4 perfectly overlay the fraction transformed data, Table 2. Note that the change required in Q is within the 95% confidence limit. The values of k we arrive at by both analysis are within an order of magnitude. This is well within the experimental error for our methodology resulting in the scatter of Figure 4.

IV. Conclusions.

The transformation kinetics and optical constants of TiO_xN_y thin films with increasing amounts of nitrogen were studied by using *in-situ* heating stage TEM and optical models. The results show that increasing the nitrogen flow up to 40% of the oxygen flow has little effect on the optical constants, increases the deposition rate and allows for more stable operation during deposition. The activation energy varies from 1.96-0.82 eV, and the crystallized phase was anatase. As nitrogen is added the mobility of Ti and O atoms is limited, and the activation energy, velocity pre-exponential, and nucleation rate decrease. The higher the nitrogen content, the higher the nucleation temperature. The kinetic variables extracted from nucleation and growth analysis of individual crystallites

agree well with the fraction transformed kinetic variables extractable from JMAK analysis. Results indicate that nitrogen makes a more disordered matrix and acts as a crystallization inhibitor.

The decrease of the growth activation energy with increasing N_2 flow is the most difficult parameter to rationalize. The value of the activation energy is typically associated with the limiting atomic transport mechanism, where with no N_2 $Q \cong 2$ eV and falls quickly to about 1 eV to 1.3 eV. The traditional explanation would be a shift to a process limited by bulk diffusion to that of grain boundary diffusion. However, there are no grain boundaries in or near the isolated growing crystallites, only single phase boundaries. It is conceivable that the increase in nitrogen content alters the rate of anion incorporation at kink sites in the ledges of the growing TiO_2 grains, which would explain the decreased activation energy.

References:

1. J. Szczyrbowski, G. Bräuer, M. Ruske, H. Schilling and A. Zmelty, *Thin Solid Films*, Vol. 351 (1999), 254-259
2. H.A. Macleod, Thin Optical filters, 2nd ed. (Adam Hilger, Bristol, 1986) 391-3
3. R. Dannenberg, Phil Greene, *Thin Solid Films,* Vol. 360 (2000) 122-127.
4. R. Dannenberg, P. Greene, 5th Int. Symp. on Sputtering and Plasma Processes (ISSP), Kanazawa, Japan, June 16±18 (1999) 116.
5. R. Dannenberg, P. Greene, SVC 42nd Annual Technical Conference Proceedings, Chicago IL, April 17±22 (1999) 23.
6. S.B. Amor, G. Baud, J.P. Besse and M. Jacquat, *Mater. Sci. Eng*. B47 (1997) 110±118.
7. A. Aidla, T. Uustare, A. -A. Kiisler, J. Aarik and V. Sammelselg, *Thin Solid Films,* Vol. 305 (1997) 270.
8. G.M. Krishna, S. Kanakaraju, S. Mohan, *Vacuum,* Vol. 46 (1995) 33.
9. A. Rizzo, L. Mirenghi, L. Tapfer, M. Alvisi, L. Vasanelli, F. Sarto and S. Scaglione, *SPIE*, Vol. 2776 392-399.
10. *Zeitschrift für Kristallographie*, Volume 136, (1972). 273
11. *Canadian Mineralogist*, Volume 017,(1979) 77
12. K. Fukushima and I. Ymada, *Nuclear Instruments and Physics Research B,* Vol. 112 (1996) 116-119
13. Ping Jin and Shigeo Maruno, *Jpn. J. Appl. Phys*. Vol. 30 No 9A (1991) 2058-62

14. A. Bittar, D. Cochrane and S. Caughley, *J. Vac. Sci. Technology A* 15(2) (1997), 223-229

15. W.A. Johnson, R.F. Mehl, *Trans.* AIME 135 (1939) 416-458

16. M. Avrami, *Journal of Chemical Physics* 7 (1939) 1103-1112

17. L.E. Levine, K. Lakshmi Narayan and K. F. Kelton, *Journal of Materials Research*, Vol. 12, No. 1, (1997) 124-132

18. Hun Seo, Tae-Hee Jeong, Jeong-Mong Park, Cheong Yeon, Sang-Jun Kim and Sang-Youl Kim, *Jpn. J. Appl. Phys*., Vol. 39 (2000) 745-51

19. J. Tauc, R. Grigorovichi, Y. Yancu, *Phys. Solid State* Vol. 15 (1966) 627.

20. Porter and Easterling, Phase transformations in metals and alloys, Chapman & Hall, 1981 p.289

Table I. Optical Properties of TiOxNy Films

N_2 to O_2 Ratio (sccm/sccm)	Thickness Angstroms	Band Gap Energy eV	At 550 nm	
			Index of refraction	Extinction coefficient
0	538.52	3.45	2.483	0.005
6.1	582.51	3.45	2.4604	0.00026
12.9	595	3.45	2.4381	0.00135
20.6	526	3.45	2.4161	0.001792
29.6	532.74	3.435	2.4031	0.001075
40	381.76	3.424	2.425	0.001801

Table II. Kinetic Parameters

N_2/O_2	n_{JMAK}	k_{JMAK} (sec^{-n}) from Equation 5	Q_{mod} (eV)	N ($um^2 sec^{-1}$)	ν_o from ν(T) ln(nm/min)	k_{kin} (sec^{-n}) from Equation 4	Q_{kin} (eV) from ν(T)	95% Confidence Limits
0.00	3.03	1.06×10^{-3}	1.961	6.64×10^{-3}	47.162	1.55×10^{-3}	1.961	-
12.90	3.00	1.07×10^{-4}	1.549	6.64×10^{-5}	30.118	1.55×10^{-5}	1.495	+/- 0.315
20.69	3.05	5.28×10^{-5}	0.823	7.27×10^{-6}	19.626	1.04×10^{-4}	0.839	+/- 0.225
29.63	2.99	1.35×10^{-6}	1.225	4.35×10^{-6}	24.691	1.45×10^{-6}	1.155	+/- 0.663

Figure 1. Deposition rate as a function of nitrogen content. As the nitrogen content is increased the operating point becomes more metallic and a higher rate is achieved.

Figure 2. Indexing of diffraction rings for as-deposited and crystallized phases. Both phases contain the same diffraction rings indicating that the same phase or phases is present. TiN and rutile phases can be safely excluded as constituents.

Figure 3. Nucleation onset temperature as a function of nitrogen content. The increased nitrogen acts as an impediment to the onset of crystallization.

Figure 4. Natural log of growth velocity as a function of reciprocal temperature. The legend indicates the N_2/O_2 Ratio.

Figure 5. Growth velocity as a function of reciprocal temperature. The legend indicates the N_2/O_2 Ratio. This is an extrapolation of the data from Figure 3 that shows the trends of each sample at high temperatures. The growth velocity for the sample with no nitrogen is significantly higher than those with nitrogen.

Figure 6. Activation energy as a function of nitrogen content. As nitrogen is added the activation energy decreases.

Figure 7. T= 730 ^{o}C Growth velocity as a function of nitrogen flow. Notice the greatly increased velocity of the sample with no nitrogen.

Figure 8. Data plotted from the fraction transformed. The legend indicates the N_2/O_2 Ratio. The intercept of each line with the y-axis indicates the *k* for that sample.

Figure 9. T= 400 ^{o}C fraction transformed for all nitrogen flows. The legend indicates the N_2/O_2 Ratio. As the nitrogen content increases the time for transformation takes longer. The kinetic variable extracted from the $f(t)$ analysis agree very well with the experimental data.

Figure 10. T= 400 ^{o}C Fraction transformed for 29.63 N_2/O_2 ratio using the kinetic variables from $f(t)$ and nucleation and growth. A change of 6% in the activation energy is enough to have the curves agree.

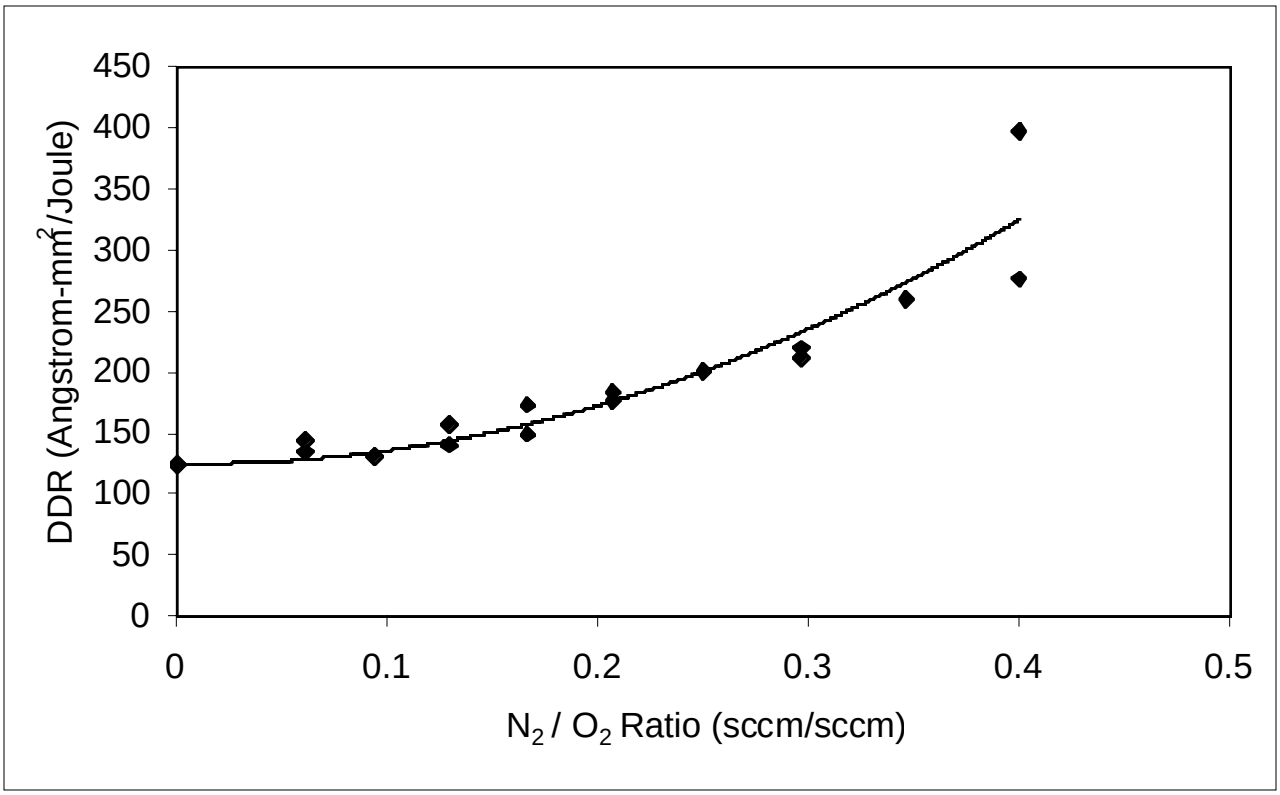
450
400
350
300
250
200
150
100
50
0
DDR (Angstrom-mm2/Joule)
0
0.1
0.2
0.3
0.4
0.5
N2 / O2 Ratio (sccm/sccm)

Figure 1.

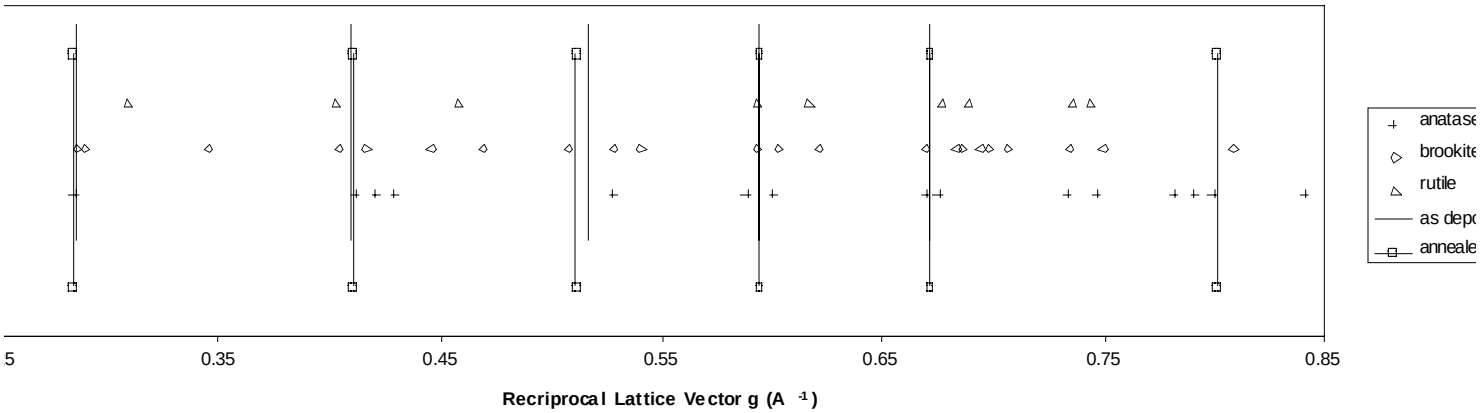
anatase
brookite
rutile
as depo
anneale
5
0.35
0.45
0.55
0.65
0.75
0.85
Recriprocal Lattice Vector g (A -1)

Figure 2.

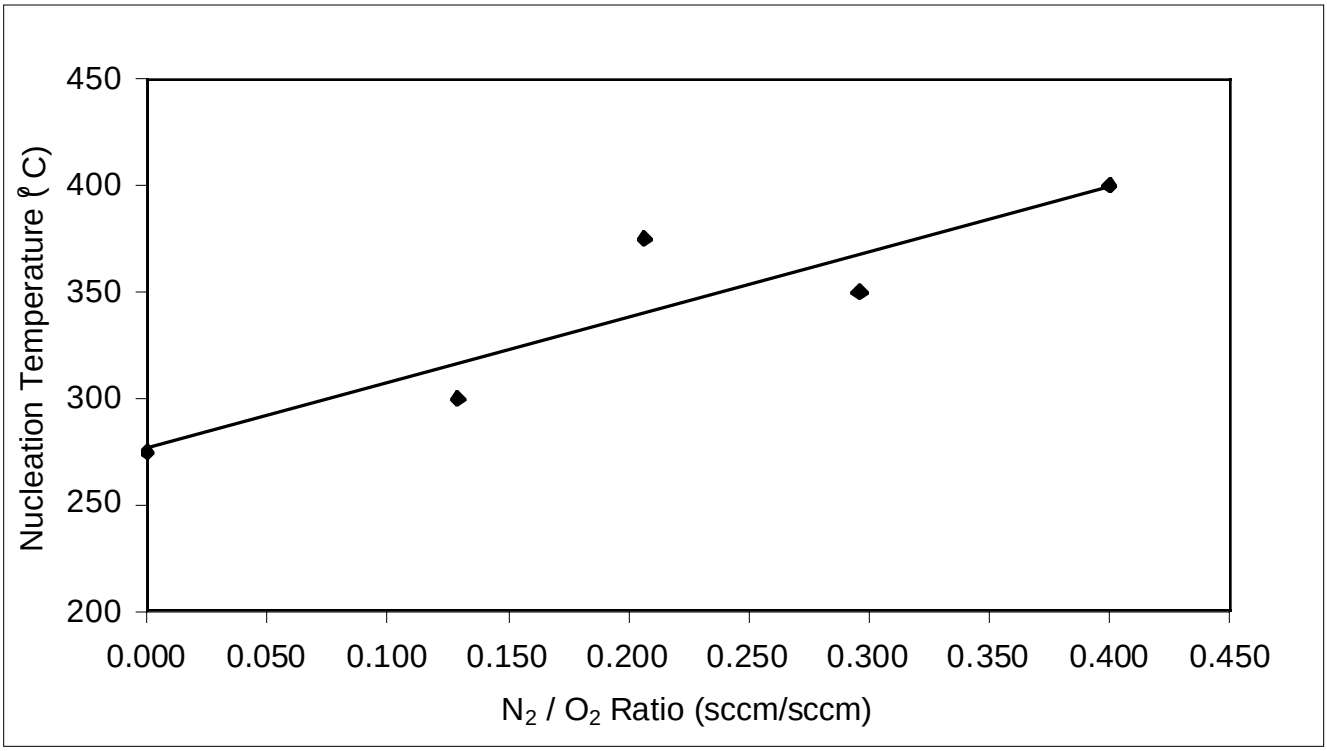
450
400
350
300
250
200
Nucleation Temperature (° C)
0.000
0.050
0.100
0.150
0.200
0.250
0.300
0.350
0.400
0.450
N2 / O2 Ratio (sccm/sccm)

Figure 3.

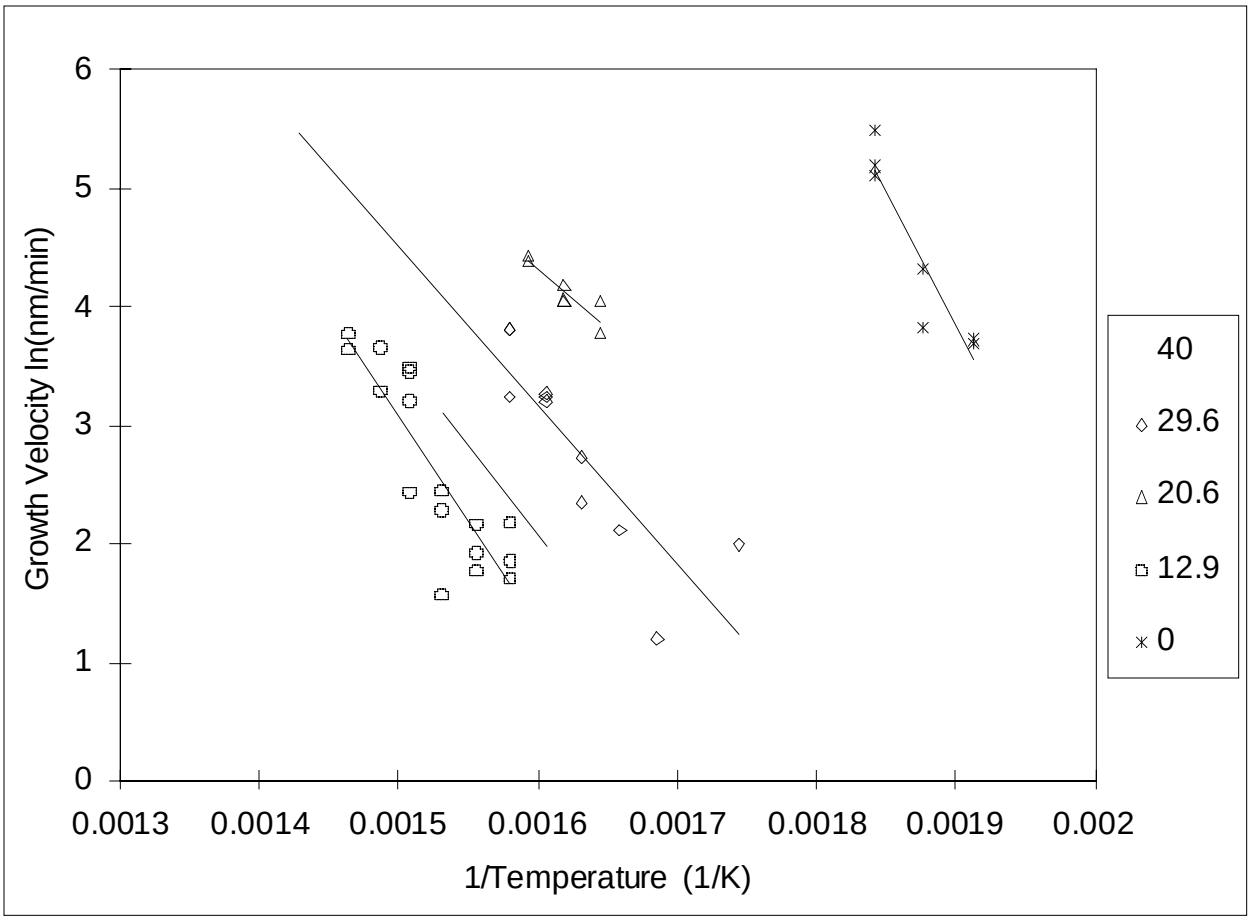
Growth Velocity ln(nm/min)
6
5
4
3
2
1
0
0.0013
0.0014
0.0015
0.0016
0.0017
0.0018
0.0019
0.002
1/Temperature (1/K)
40
29.6
20.6
12.9
0

Figure 4.

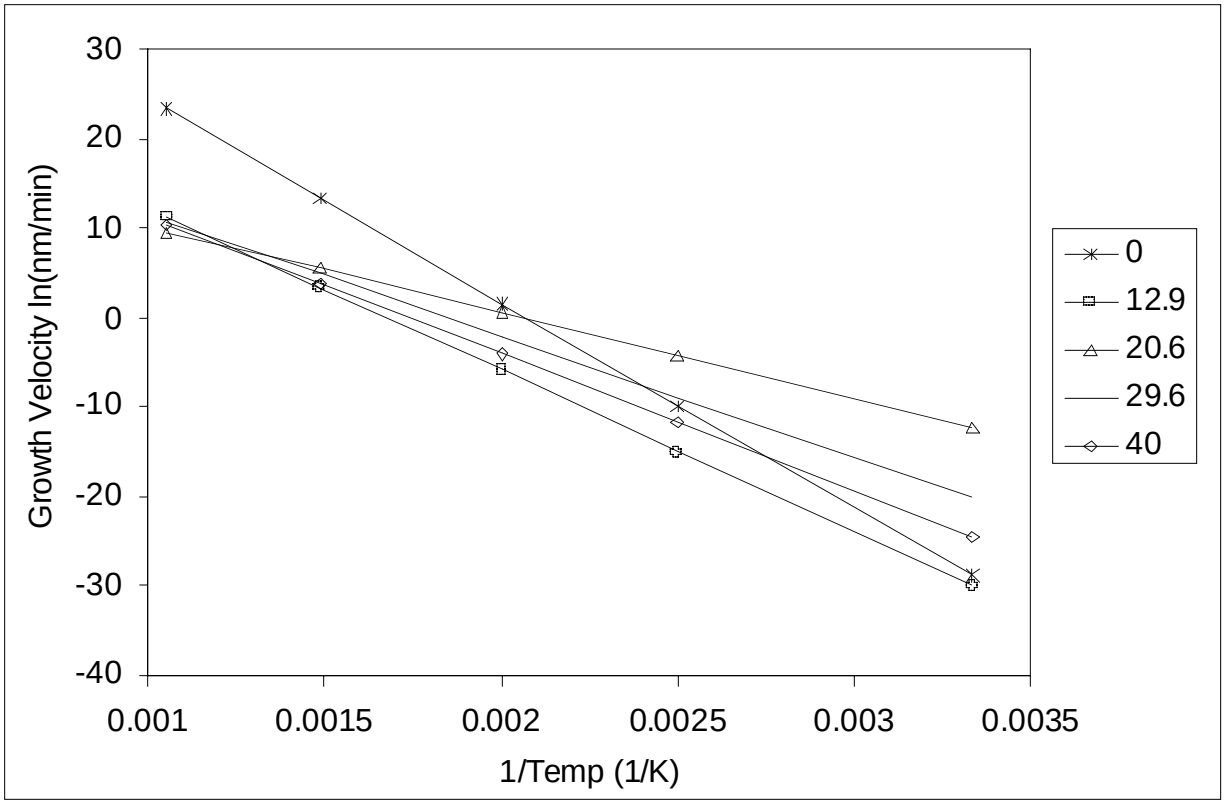
30
20
10
0
-10
-20
-30
-40
Growth Velocity ln(nm/min)
0.001
0.0015
0.002
0.0025
0.003
0.0035
1/Temp (1/K)
0
12.9
20.6
29.6
40

Figure 5.

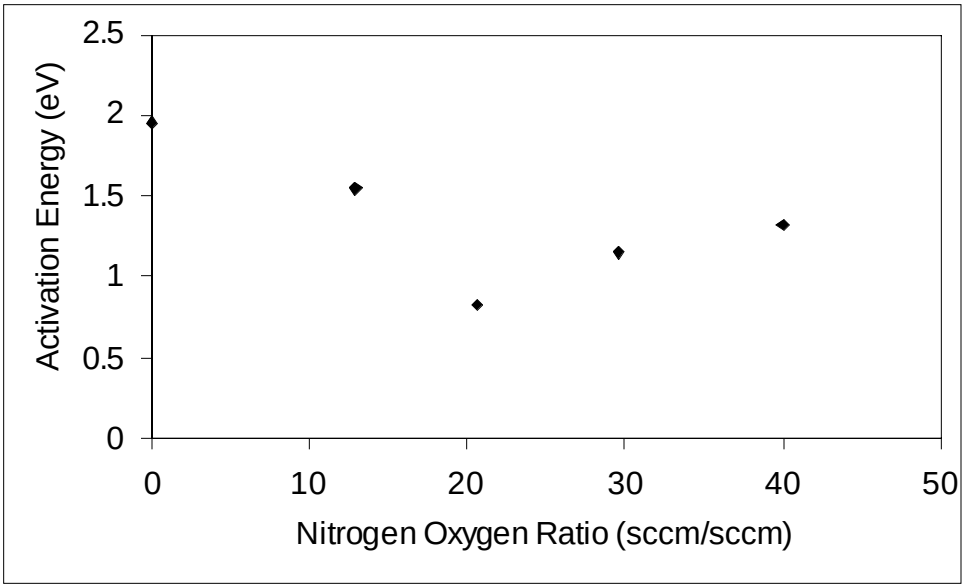
Activation Energy (eV)
2.5
2
1.5
1
0.5
0
0
10
20
30
40
50
Nitrogen Oxygen Ratio (sccm/sccm)

Figure 6.

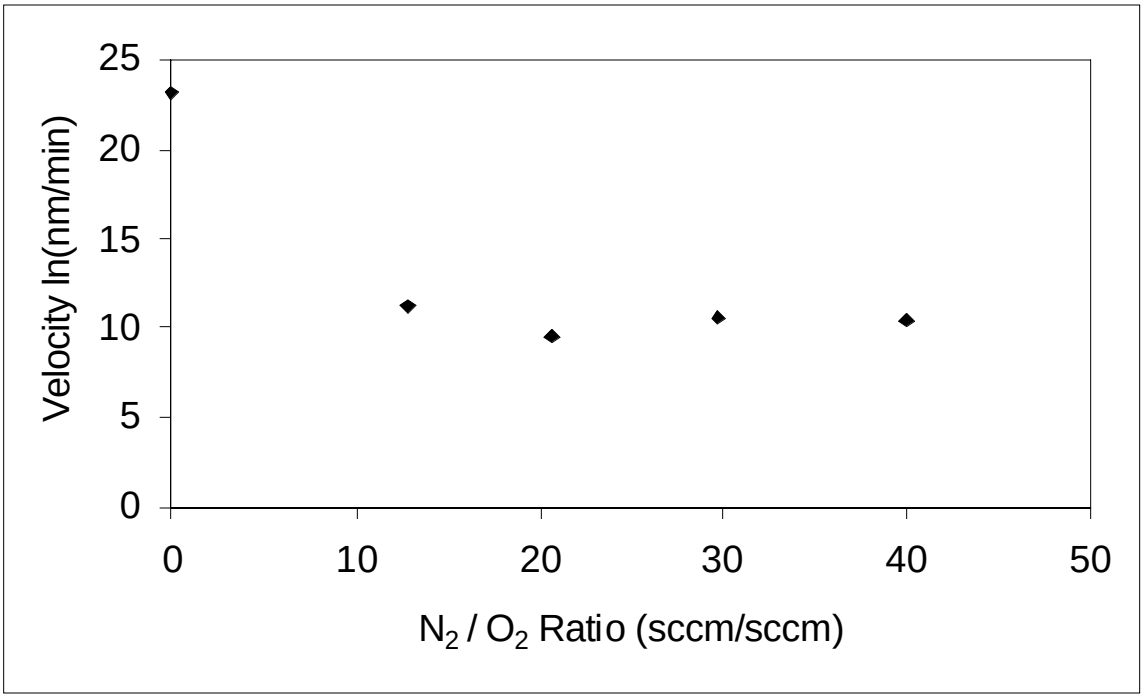
25
20
15
10
5
0
Velocity ln(nm/min)
0
10
20
30
40
50
N2 / O2 Ratio (sccm/sccm)

Figure 7.

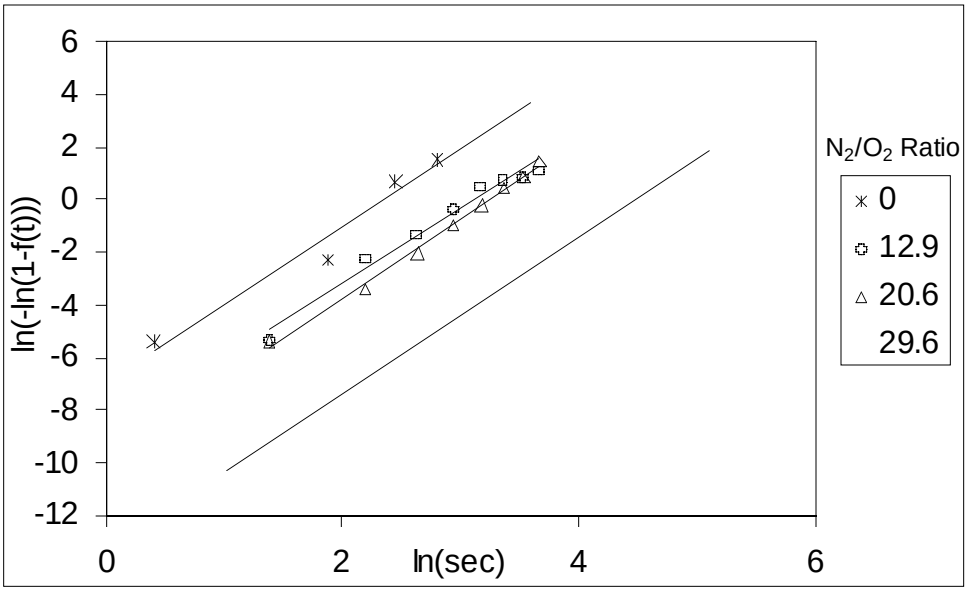

Figure 8.

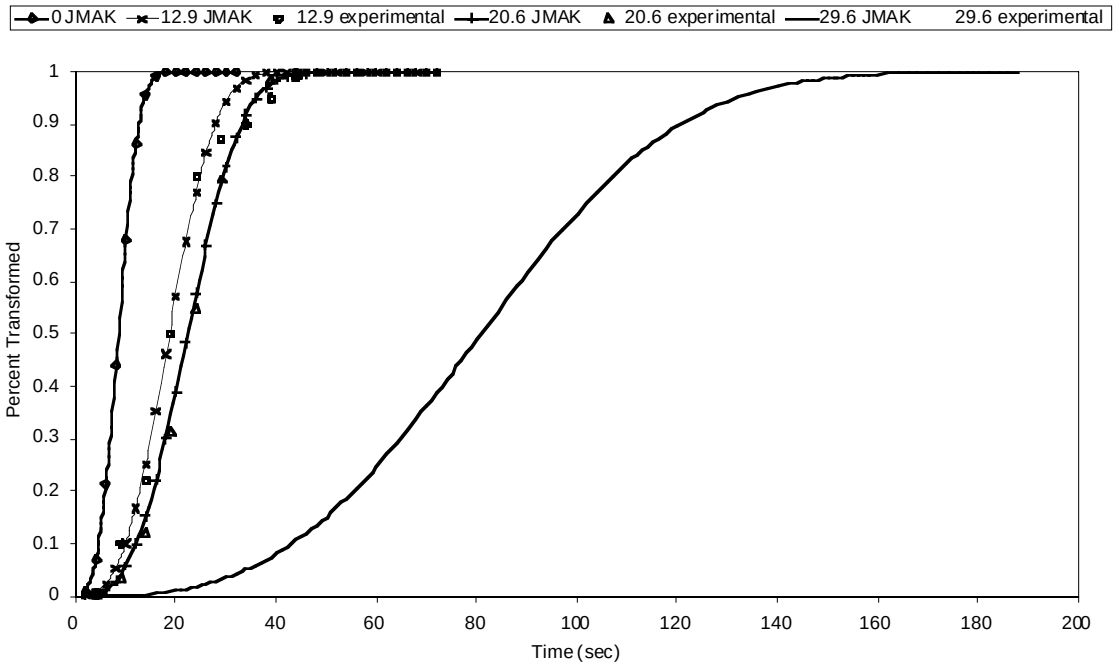
0 JMAK
12.9 JMAK
12.9 experimental
20.6 JMAK
20.6 experimental
29.6 JMAK
29.6 experimental
Percent Transformed
Time (sec)
0
0.1
0.2
0.3
0.4
0.5
0.6
0.7
0.8
0.9
1
0
20
40
60
80
100
120
140
160
180
200

Figure 9.

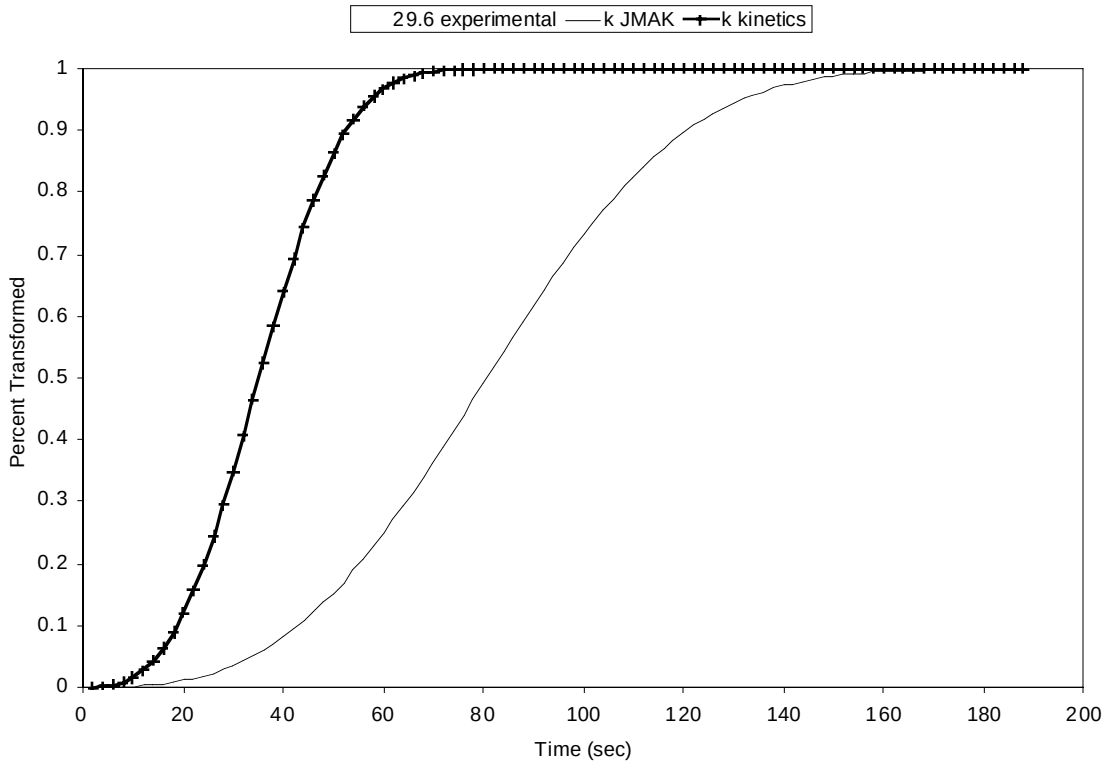
29.6 experimental
k JMAK
k kinetics
Percent Transformed
Time (sec)
0
0.1
0.2
0.3
0.4
0.5
0.6
0.7
0.8
0.9
1
0
20
40
60
80
100
120
140
160
180
200

Figure 10.